10.2514/6.2016-1322

AIAA SciTech Forum
4-8 January 2016, San Diego, California, USA
15th Dynamics Specialists Conference

Nonlinear Thermal Reduced Order Models for a Hypersonic Vehicle

Ryan J. Klock[1] and Carlos E.S. Cesnik[2]
University of Michigan, Ann Arbor, MI 48109-2140

A set of reduced order models are considered to determine the variation of the material thermal capacity and thermal conductivity with respect to temperature for a representative hypersonic vehicle structure on a terminal trajectory. The number of thermal degrees of freedom is first reduced by projecting the thermal state of a sample structure into a modal space whose bases are determined using proper orthogonal decomposition. A numerical integration scheme based on the Crank–Nicolson algorithm is used to simulate the thermal state forward in time. Models for the generalized material thermal properties are based on the method of Kriging, a least-squares polynomial approximation, and a singular value decomposition approach. The resulting thermal models are compared in terms of accuracy and computational efficiency. The singular value decomposition approach is shown to be the superior overall reduced-order model to capture the variation of thermal properties with temperature when compared to a full-order finite element solution.

I. Introduction

HIGH speed weapons systems, particularly hypersonic vehicles, operate in a high energy environment characterized by strong fluid, thermal, and structural interactions. Due to a lack of ground test facilities which can generate the high energy environment of interest, the primary focus for hypersonic vehicle design and preliminary evaluation must be through analytical and computational simulations. Current computational research efforts have focused on either improving particular physics model fidelity with limited discipline interactions due to a high computational cost, or including many discipline interactions using very simple models. Thus, there is a wide middle-ground between the low-fidelity, high-interaction and high-fidelity, low-interaction modeling regimes that has yet to be considered, but is critical to the development of high speed weapons systems.

In this work, a scramjet propelled hypersonic vehicle was considered. Scramjets are a form of high-speed air-breathing jet engine which utilizes the shape of the vehicle forebody, engine inlet, and engine flowpath to compress, combust, and exhaust fuel and air to produce thrust at speeds above Mach 5. To operate a scramjet, its host vehicle must be flown at conditions of high dynamic pressure, leading to trajectories of relatively low altitudes and high speeds for an air-breathing vehicle. Under such flight conditions, aerodynamic heating becomes a driving factor in the design as high surface temperatures and heat flux seep into the structure and modify the elastic characteristics of the vehicle. Critical to accurate determination the thermal state of the structure is consideration of the variation of the material thermal properties with temperature, specifically thermal conductivity and heat capacity.

Past work by Falkiewicz and Cesnik[1,2] had demonstrated that reduction of the thermal problem is possible by identification of appropriate basis modes and projection of the governing equations into the space spanned by these modes. Modal identification using proper orthogonal decomposition (POD)[1], specifically through the method of snapshots, was used to derive orthogonal thermal basis modes which could then be linearly combined to approximate the temperature distribution of a structure. Throughout much their analysis, the thermal state of the structure was integrated numerically using a Crank–Nicolson scheme to determine the thermal basis coordinates. However, either do to an assumption that the temperature range was insufficient to vary the material thermal properties, a lack of material property data, or simply neglect, the variation of the thermal conductivity and heat capacity of the materials was not considered.

The variation of material thermal properties has been considered in other literature, although often in a limited capacity. In a study by McMasters et al.[3] of nonlinear thermal diffusion, an exact analytical solution was derived with a thermal conductivity which varied linearly with temperature and was later used to verify the results of a finite

[1] Graduate Research Assistant, Department of Aerospace Engineering, rjklock@umich.edu
[2] Professor, Department of Aerospace Engineering, AIAA Fellow, cesnik@umich.edu

element thermal analysis code, CALORE. While thermal conductivity was variable, all other thermal properties were assumed to be constant.

Matney et al.[4] considered the variation of thermal properties for the problem of hypersonic flow over a panel with underlying stiffeners in the development of an adaptive thermal basis set. In their study, aerodynamic pressure was modeled using piston theory[26] and heat flux was modeled using the Eckert reference enthalpy method.[27] These aerodynamic and thermal loading solutions where then applied to a finite element model (FEM) to observe structural and thermal responses. Variation of the in-plane thermal conductivity with respect to the temperature of the panel was modeled using a property lookup table. Each element of their panel FEM was identical and could use the same lookup table for all elements. This approach to modeling the variation of material thermal properties with respect to temperature was therefore limited to very simple geometries where uniform finite elements could be used.

For the study presented in this paper, a representative substructure of the hypersonic vehicle developed by Pasiliao et al. [5] using the Preliminary Aerothermal Structural Simulation (PASS) code suite was considered. This vehicle is an air-launched, rocket-scramjet combined cycle propelled vehicle, which performs a three-phase trajectory. Shown in Figure 1, the vehicle would first boost under rocket propulsion up to a cruising altitude above 50 kft (15.2 km) and airspeed above Mach 5. The rocket booster would then be jettisoned and a scramjet propulsion system engaged to maintain a mostly steady and level cruise condition. Finally, after exhausting the scramjet fuel supply, the vehicle would enter an unpropelled terminal phase to reach a ground target some distance downrange.

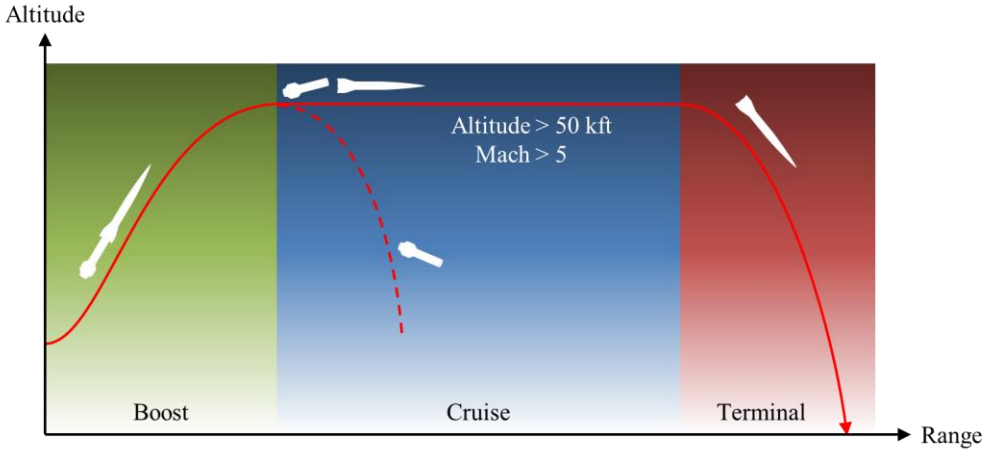

Figure 1: Basic outline of a boost-cruise-terminal mission profile for an air-launched, rocket-boosted hypersonic vehicle

Witeof and Neergaard[6] performed material trade and sizing optimization studies of thermal protection systems (TPS) and structural elements to minimize mass while satisfying material temperature and stiffness constraints. In their trade study, aerodynamic heating was approximated using the Aerothermal Target Analysis Program (ATAP).[7] Structural modes were approximated using Timoshenko beam elements and the variation in modal frequencies due to thermal effects was investigated with respect to flight time.

The thermal state of the vehicle in the terminal phase is the main focus of this paper. In this phase, the highest structural temperatures are experienced and are most likely to impact the flight characteristics of the vehicle. It is also in this phase that an accurate model of the vehicle state is required to maximize strike accuracy and therefore effectiveness as a high-speed weapon. To first reduce the order of the thermal problem, the method of POD is applied and the governing equations generalized with the resulting basis set. Then, to capture the influence of structural temperature on thermal conductance and capacitance, three reduced-order models (ROMs) were investigated: least-squares fit multi-dimensional polynomials, the method of Kriging, and a newly developed method based on a combination of singular value decomposition[28] and linear correlation.

II. Theoretical Development

A. Proper Orthogonal Decomposition

A common method to reduce the dimensionality of the thermal problem is to apply proper orthogonal decomposition (POD). POD is a statistical method in which empirical data is used to identify correlated features, or modes, of a system and is optimal in the sense that the fewest number of modes may be used to represent the majority of the system energy. The retention of only the most dominant modes allows for the creation of a basis that captures the overall behavior of the system while significantly reducing the number of degrees of freedom. The ultimate goal is then to represent the thermal state of a system as a sum of basis modes and time varying coefficients, i.e.,

$$\mathbf{T}(t) = \boldsymbol{\Psi}\mathbf{c}(t), \tag{1}$$

where $\mathbf{T}(t)$ is a column vector of time-varying temperatures at predefined locations of interest such as finite element nodes, centroids, or integration points, $\boldsymbol{\Psi}$ is the thermal basis matrix whose columns are the thermal basis modes, $\mathbf{c}(t)$ is a column vector of the time varying coefficients for each basis mode, and t is time. The basis matrix $\boldsymbol{\Psi}$ is determined by consideration of a snapshot matrix $\mathbf{A}$ whose columns are vectors of temperatures at specific moments during a high-fidelity heat-transfer simulation, such as an FEA solution. The error incurred by representing the thermal state with a truncated thermal basis matrix may be interpreted as the relative energy lost ε_{rel} by projecting the snapshot matrix $\mathbf{A}$ onto the space spanned by the truncated thermal basis matrix $\boldsymbol{\Psi}$, given by[39]

$$\varepsilon_{rel} = \frac{\left\|\mathbf{A} - \boldsymbol{\Psi}\boldsymbol{\Psi}^T\mathbf{A}\right\|^2}{\left\|\mathbf{A}\right\|^2} \ . \tag{2}$$

For brevity, a full description of the POD method is omitted, however a thorough description of this method's application to thermal problems is given in Ref. [1].

B. Generalization of Thermal Problem

Once an appropriate thermal basis is determined, one may generalize the governing system of equations for the thermal problem

$$\mathbf{M}\left(\mathbf{T}(t)\right)\dot{\mathbf{T}}(t) + \mathbf{K}\left(\mathbf{T}(t)\right)\mathbf{T}(t) = \mathbf{F}(t), \tag{3}$$

into

$$\mathbf{m}\left(\mathbf{c}(t)\right)\dot{\mathbf{c}}(t) + \mathbf{k}\left(\mathbf{c}(t)\right)\mathbf{c}(t) = \mathbf{f}(t), \tag{4}$$

where

$$\mathbf{m}\left(\mathbf{c}(t)\right) = \boldsymbol{\Psi}^T\mathbf{M}\left(\boldsymbol{\Psi}\mathbf{c}(t)\right)\boldsymbol{\Psi}, \tag{5a}$$

$$\mathbf{k}\left(\mathbf{c}(t)\right) = \boldsymbol{\Psi}^T\mathbf{K}\left(\boldsymbol{\Psi}\mathbf{c}(t)\right)\boldsymbol{\Psi}, \tag{5b}$$

$$\mathbf{f}(t) = \boldsymbol{\Psi}^T\mathbf{F}(t), \tag{5c}$$

and where $\mathbf{M}(\mathbf{T})$ and $\mathbf{K}(\mathbf{T})$ are the thermal capacity and conductivity matrices, each a function of the time varying temperature vector $\mathbf{T}(t)$, and $\mathbf{F}(t)$ is the time varying thermal load vector.

C. Numerical Integration

To numerically integrate the generalized thermal problem forward at discrete times t_n and t_{n+1}, separated by the time interval Δt, the Crank-Nicolson algorithm is considered due to its known unconditional stability for both linear and nonlinear heat conduction systems.[30] This results in:

$$\mathbf{c}(t_{n+1}) = \left[\frac{\mathbf{k}}{2} + \frac{\mathbf{m}}{\Delta t}\right]^{-1} \left\{\left[-\frac{\mathbf{k}}{2} + \frac{\mathbf{m}}{\Delta t}\right]\mathbf{c}(t_n) + \frac{\mathbf{f}(t_n) + \mathbf{f}(t_{n+1})}{2}\right\}. \tag{6}$$

D. Modeling Temperature Dependent Material Thermal Properties

1. Least-Squares Fit Polynomials

The first method considered is to approximate each entry of the generalized thermal matrices using polynomials formed from the thermal mode coordinates, i.e.

$$\mathbf{B} \approx \mathbf{R}_{ls}\left[1 \quad \cdots \quad 1 \quad c_1 \quad \cdots \quad c_r \quad c_1c_1 \quad c_1c_2 \quad \cdots \quad c_rc_r \quad c_1c_1c_1 \quad c_1c_1c_2 \quad \cdots\right]^T = \mathbf{R}_{ls}\bar{\mathbf{c}}, \tag{7}$$

where $\mathbf{R}_{ls}$ is a matrix of coefficients for each permutation of thermal mode coordinates c_i, where i varies from 1 to r for each thermal basis, and $\mathbf{B}$ contains the entries of the thermal matrices $\mathbf{k}$ and $\mathbf{m}$ stored as column vectors

$$\mathbf{B} = \begin{bmatrix} k_{1,1} & k_{1,2} & \cdots & k_{r,r} & m_{1,1} & m_{1,2} & \cdots & m_{r,r} \end{bmatrix}^T. \tag{8}$$

The coefficient matrix $\mathbf{R}_{ls}$ is determined by the solution to the least-squares problem:

$$\mathbf{R}_{ls} = \left(\bar{\mathbf{c}}\bar{\mathbf{c}}^T\right)^{-1}\bar{\mathbf{c}}\bar{\mathbf{B}}, \tag{9}$$

where $\bar{\mathbf{c}}$ is a matrix whose columns are vectors of the thermal mode coordinates for each snapshot expanded to include all powers and combinations of the modal coordinates desired for the polynomial to be fit and $\bar{\mathbf{B}}$ is a matrix whose columns are vectors of the entries of the thermal matrices $\mathbf{k}$ and $\mathbf{m}$ corresponding to each set of thermal coordinates.

2. Kriging

The second method considered to capture the variation of the thermal capacity and conductivity matrices with respect to the thermal modal coordinates, $\mathbf{m}(\mathbf{c})$ and $\mathbf{k}(\mathbf{c})$, is Kriging.[10] Kriging is a statistics-based method that can incorporate the trend model properties of a more typical linear or polynomial regression with the spatial correlation properties of kernel-based approximation methods.[14] It provides flexible and computationally efficient models that may be adapted to represent many complex *n*-dimensional response surfaces. Kriging is a useful approximation of computer analysis in particular, where no random error is present, due to the method's ability to exactly recover the solutions of the training points used to create it.

To create the Kriging model, a set of training samples of thermal conductivity and capacity matrices is produced from a heat-transfer FEM based on coordinates of the thermal modal basis. Selection of the modal coordinates is determined by Latin hypercube sampling[29] (LHS) within thermal coordinate bounds determined by the extremes observed in the POD snapshot matrix previously described. Upon collection of a number of model training and testing samples, several Kriging models may be constructed based on different combinations regression and correlation functions, many of which are available in the Matlab® DACE Toolbox.[31] Each model is then tested for accuracy in reproducing the test samples by a root-mean-squared-error (RMSE) and maximum normalized error (Norm L_∞).

3. Singular Value Decomposition

The third method is a new approach which uses singular value decomposition (SVD) and linear correlation. This method is modeled after Ref. [13] which used a similar approach to efficiently approximate the aerodynamic loads of a maneuvering aircraft. For the application of determining the entries of the generalized thermal capacity and conductivity matrices, a sampling of the FEM solutions is first required. These are taken using the same LHS as the Kriging ROM generation for direct comparison of the methods. A snapshot matrix $\bar{\mathbf{B}}$ is constructed with the entries of $\mathbf{k}(c)$ and $\mathbf{m}(c)$ as column vectors at each LHS point and may be represented as

$$\mathbf{U}\boldsymbol{\Sigma}\mathbf{V}^T = \bar{\mathbf{B}}, \tag{10}$$

where $\mathbf{U}$ is a square matrix whose columns are the left singular vectors of $\bar{\mathbf{B}}$, $\boldsymbol{\Sigma}$ is a rectangular diagonal matrix of the singular values, and $\mathbf{V}$ is a square matrix whose columns are the right singular values of $\bar{\mathbf{B}}$. Because of the arrangement of the snapshot matrix $\bar{\mathbf{B}}$, $\mathbf{U}$ may be thought of as a set of orthogonal unit vectors which span the space populated by the snapshots, $\boldsymbol{\Sigma}$ as the relative importance of each unit vector to describing that space, and $\mathbf{V}$ as a list of coefficients corresponding to the location of each snapshot in the space.

If the space spanned by the columns of $\bar{\mathbf{B}}$ is large, i.e. each snapshot contains a large number of degrees of freedom, the problem may be reduced by removing the smallest singular values in $\boldsymbol{\Sigma}$ as well as the corresponding columns of $\mathbf{U}$ and $\mathbf{V}$. In this way, dimensions of the snapshots which are least important to the representation of $\bar{\mathbf{B}}$ may be ignored while and the order of the eventual model is reduced.

The next step is to relate the coordinates of each snapshot stored in $\mathbf{V}$ to the thermal coordinate inputs $\bar{\mathbf{c}}$. A correlation matrix $\mathbf{R}_{svd}$ is determined which relates the basis amplitudes in $\mathbf{V}$ to the thermal mode coordinates for each snapshot stored as column vectors in matrix $\bar{\mathbf{c}}$ using a least-squares fit

$$\bar{\mathbf{c}}^T\mathbf{R}_{svd} = \mathbf{V} \tag{11}$$

$$\mathbf{R}_{svd} = \left(\bar{\mathbf{c}}\bar{\mathbf{c}}^T\right)^{-1}\bar{\mathbf{c}}\mathbf{V}. \tag{12}$$

Then, given any additional set of thermal mode coordinates $\tilde{\mathbf{c}}$, not necessarily included in the snapshot matrix, an estimated snapshot matrix $\tilde{\mathbf{B}}$ may be found by

$$\tilde{\mathbf{B}} = \mathbf{U}\boldsymbol{\Sigma}\mathbf{R}_{svd}^T\tilde{\mathbf{c}} \tag{13}$$

such that the columns of $\tilde{\mathbf{B}}$ contain approximate entries of the thermal matrices $\mathbf{k}$ and $\mathbf{m}$. Thus $\mathbf{k}(\mathbf{c})$ and $\mathbf{m}(\mathbf{c})$ are readily available during integration of the thermal problem.

III. Test Case

A. Structural Model

To compare each ROM approach, a sample FEM was established which was representative of a small portion of the hypersonic vehicle proposed by Pasiliao et al.[5] and later refined by Witeof and Neergaard.[6] This substructure was located at the interface of the vehicle nose ballast and fore-body, on the Earth-facing side during typical flight conditions, in a region that was previously shown in Ref. [23] to experience high thermal loads and also contain several different materials. For simplicity, this substructure was considered to be approximately 2D, despite the curvature of the vehicle's body in this region. The vehicle, sample substructure, and FEM grid are shown in Figure 2. The FEM consisted of 6478 nodes and 3040 linear hexahedral solid elements clustered near regions where high temperature gradients were expected due to external heat flux or material interfaces. Three materials are considered: elemental tungsten in the nose ballast, Exelis Inc.'s Acusil-II® material in the thermal protection layer covering the fore-body, and titanium alloy Ti-6Al-4V which comprised the structural monocoque of the vehicle. For simplicity, neighboring materials were considered to be perfectly bonded and no joiner or fastener geometry was included.

B. Material Thermal Properties

Experimental thermal properties of the materials considered in the FEM are given in Figure 3. Only one data point was available for the specific heat capacity of the Acusil-II® material to its proprietary nature. However with all other thermal properties over the temperature range of interest, the substructure and material set presented a highly nonlinear system on which to compare the thermal ROM approaches.

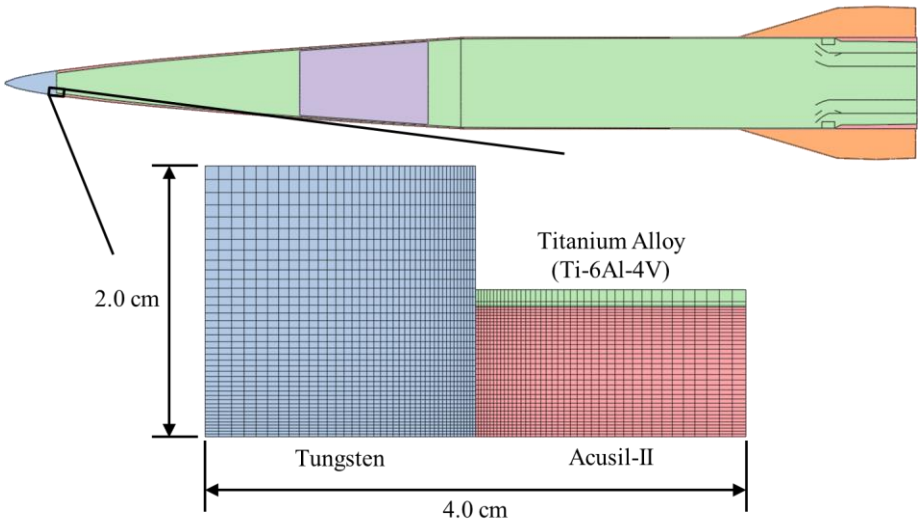

Figure 2: Sample substructure with overlaid FEM grid and its location on the vehicle

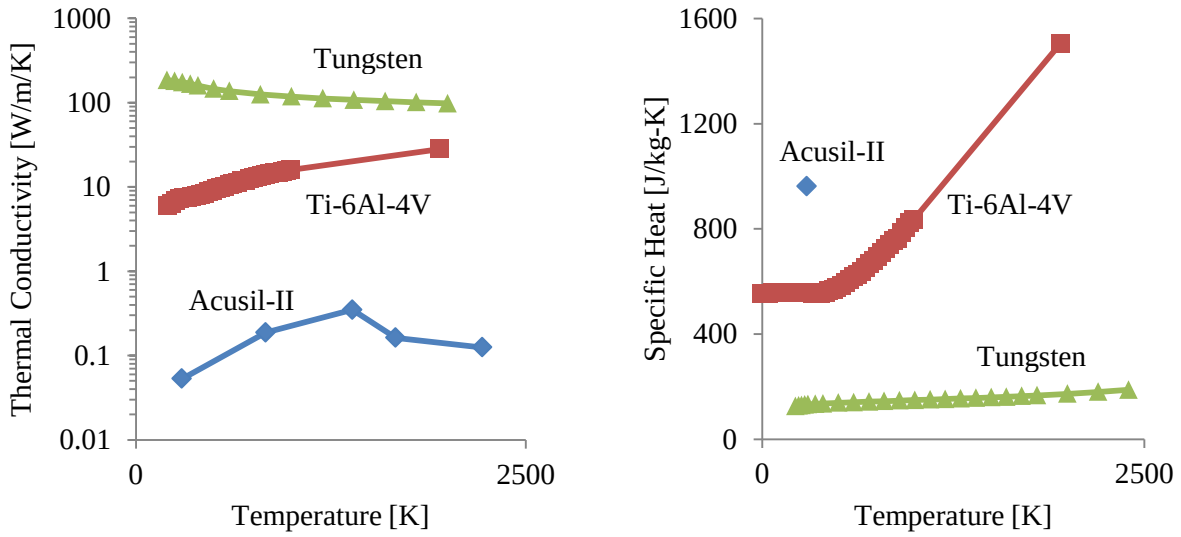

Figure 3: Large variation of thermal properties due to temperature, Refs. [15-22]

C. Sample Collection

To create the thermal property ROMs, a number of training and testing samples were required. The process used to collect these samples is outlined in Figure 4 and begins with considering the thermal bases $\boldsymbol{\Psi}$ and thermal mode ranges $\min(\mathbf{c})$ and $\max(\mathbf{c})$ resulting from a POD of an FEA heat transfer simulation of the substructure. Latin hypercube sampling was used to determine a uniformly random set of thermal coordinates $\mathbf{c}$ which were then converted to physical temperature distributions $\mathbf{T}$ within the FEM. These were then passed to an FEA solver which assembled the full thermal property matrices $\mathbf{M}$ and $\mathbf{K}$, which were then exported and generalized according to the thermal bases $\boldsymbol{\Psi}$ into $\mathbf{m}$ and $\mathbf{k}$. Each generalized thermal property matrix was then paired with its corresponding thermal coordinates $\mathbf{c}$ and sent to each of three ROM training functions to be incorporated into a thermal property ROM.

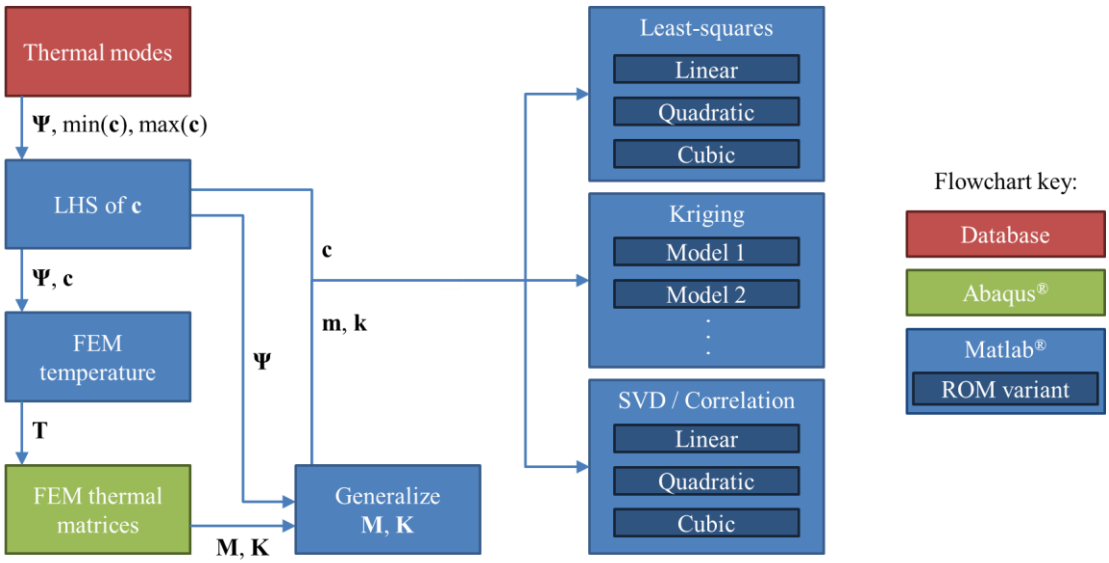

Figure 4: Training sample collection process

Within each ROM training function the $\mathbf{c}$, $\mathbf{m}$, $\mathbf{k}$ samples are divided into two groups. One group of n training samples was used to train each model within the ROM type. For the least-squares ROM, three models were considered: linear, quadratic, and cubic polynomials of the thermal coordinates $\mathbf{c}$. The Kriging ROM contained eighteen combinations of three regression functions: constant, linear, and quadratic polynomials and six correlation functions: pure exponential, general exponential, Gaussian, linear, spherical, and spline. Each of these regression and correlation functions were default forms provided with the Matlab® DACE toolbox.[31] The SVD and linear correlation ROM contained three models: linear, quadratic, and cubic polynomials of the thermal coordinates.

Another group of k testing samples was then used to test the accuracy of each model in prediction of samples not contained in the training set. The model which contained the least single entry maximum error (L_∞) normalized by the value each entry was considered the most accurate and exported for comparison against the other ROM types. The L_∞ error metric was selected to compare the different ROM variants within a training function since it is the most conservative measure of error. A flowchart of this process is shown in Figure 5.

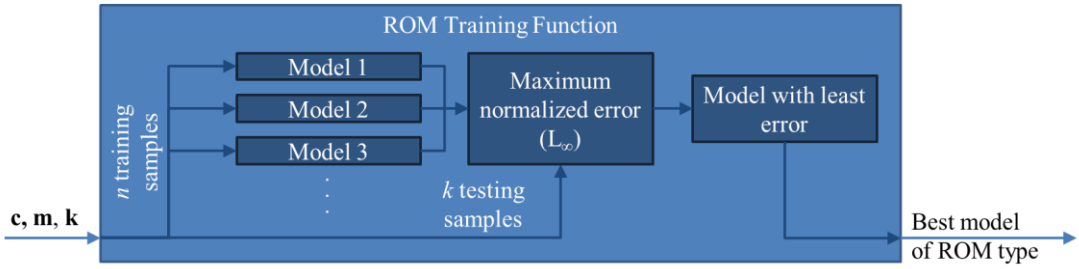

Figure 5: ROM training, testing, and selection for each ROM type

IV. Results and Discussion

A. FEA Heat Transfer Simulation

To determine a suitable POD basis set for the substructure, a high-fidelity heat transfer simulation was performed using the Dassault Systèmes Inc.'s Abaqus® FEA heat transfer solver. During simulation, at every time step the wall temperature T_w, time t, and spatial locations x, y, z of every node exposed to flow were exported to a Fortran user-defined subroutine and used to search for a corresponding node in a preprocessed database of flow conditions; namely pressure p_e, temperature T_e, and Mach number M_e. This database was determined *a priori* by an in-house unsteady aerodynamics code employing oblique shock, Prandtl-Meyer expansion, and third-order piston theory.[26] The flight trajectory consisted of a 520 second, Mach 6, 75 kft (22.9 km) altitude cruise phase during

which the vehicle was trimmed for propelled steady and level flight, followed by a 37.5 second unpropelled terminal phase along a path optimized for maximum final kinetic energy. Details of this trajectory and optimization process may be found in Ref. [23]. Once the flow properties near a node of interest were found, the Eckert reference temperature[27] and black-body radiation methods were used to determine the heat flux $\dot{q}_w$ to the node. The heat flux was imported back to the FEA heat transfer solver as a boundary condition and the solution was moved ahead in time. A flowchart of this process is shown in Figure 6.

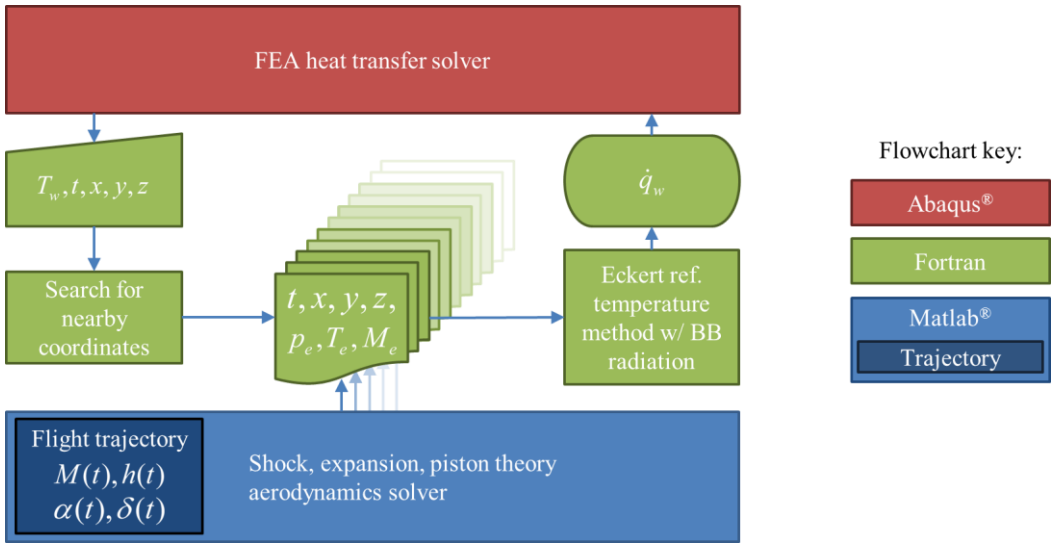

Figure 6: FEA heat transfer simulation along flight trajectory

The resulting temperature profiles of the substructure during the cruise and terminal phases are shown in Figure 7 and Figure 8, respectively.

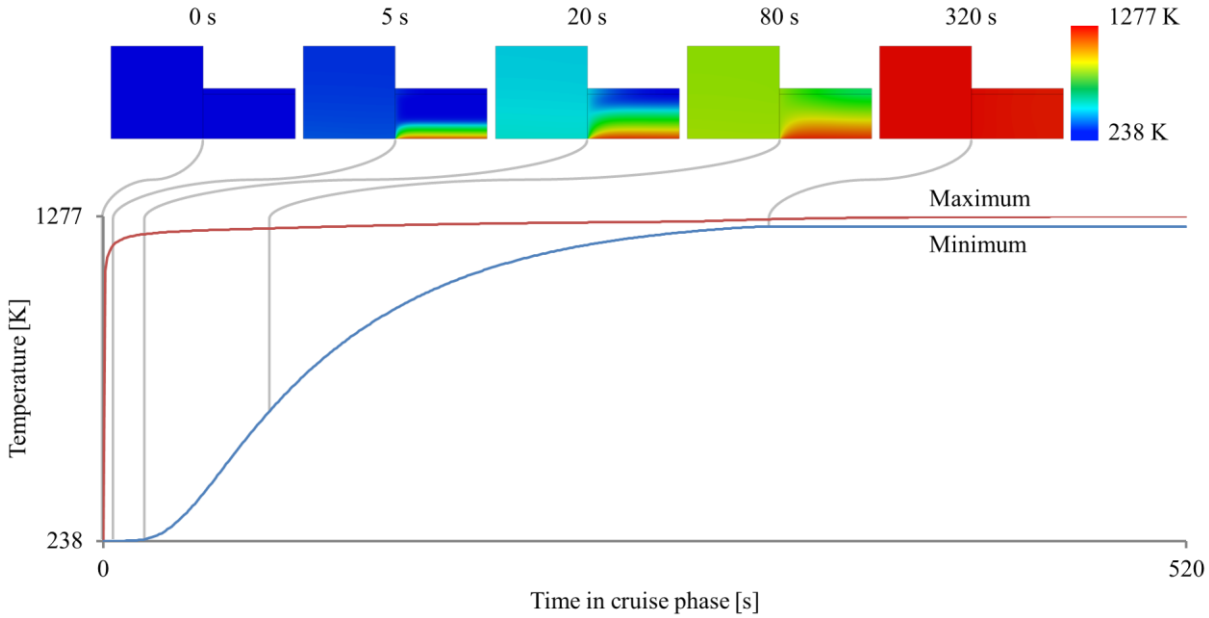

Figure 7: Temperature range in substructure during cruise phase

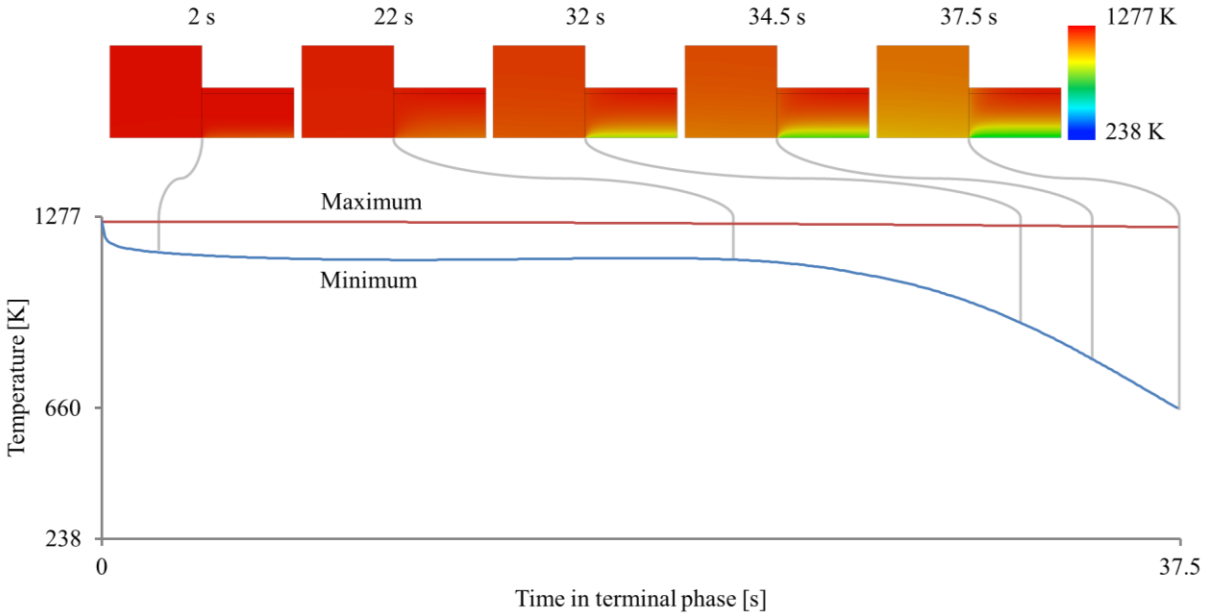

Figure 8: Temperature range in substructure during terminal phase

During the cruise phase, the substructure is initially a uniform 238 K. The outer surface of the TPS quickly warms to nearly 1277 K and begins slowly conducting heat inward toward the skin. The ballast meanwhile has a high thermal conductivity and warms almost uniformly. Protected by the TPS, the skin is the slowest to warm, however after roughly 320 s the substructure became completely thermally soaked, meaning nearly a uniform 1277 K. Upon entering the terminal phase, the vehicle switched from a nose-up to a nose-down angle of attack. Thus the substructure which was initially on the highly thermal loaded windward side of the vehicle was then on the less loaded leeward side which caused as a small initial drop in the outer TPS temperature. After about 32 s, the vehicle had sufficiently slowed to allow additional cooling of the TPS until the end of the terminal phase at 37.5 s. Throughout the terminal phase the skin remained nearly at 1277 K since insufficient time passed to conduct its heat back out through the TPS.

B. Thermal Bases

After performing a simulation of the sample structure along the cruise and terminal phase trajectories, thermal bases were determined using the method of POD. The first 5 bases are shown in Figure 9 with the relative eigenvalue magnitudes and basis truncation error shown in Figure 10. Figure 9 reveals that almost the entirety of all modes focus on describing the temperature gradient in the TPS of the model due to the low conductivity of the Acusil-II® material compared to the tungsten and titanium alloy of the ballast and skin, respectively. Some detail is afforded for the titanium alloy skin; however this is largely to enforce the temperature continuity between the skin and TPS. Despite placing almost all focus on the TPS, Figure 10 shows that the truncation of the bases to the first 5 modes provided a relative error of $\sim 10^{-8}$, which is typically sufficient to accurately represent the thermal state of the structure. Thus, one may use these bases to generalize the rank 6478 thermal problem considered by the FEA to a rank 5 problem and be confident that reasonable solution accuracy may still be obtained if similar thermal loading is simulated.

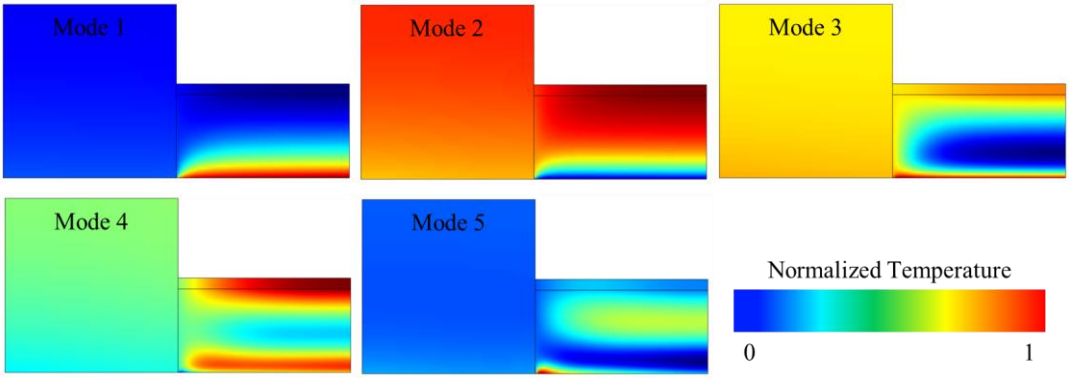

Figure 9: First 5 most prominent POD thermal modes

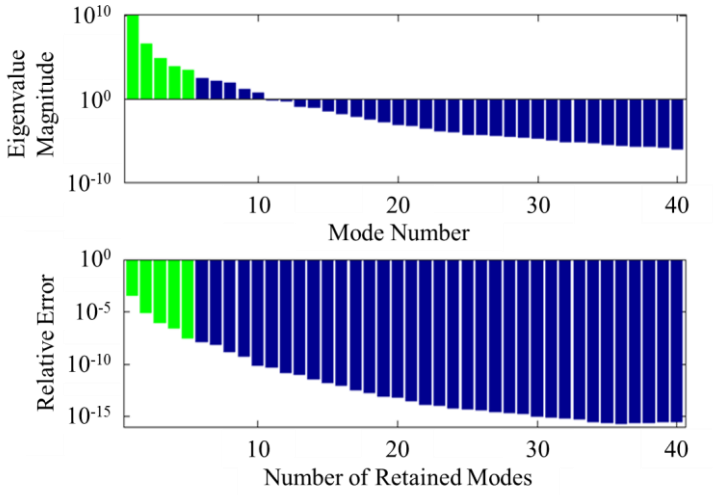

Figure 10: Relative POD eigenvalue magnitude and truncation error (green bars associated with the first 5 most prominent POD thermal modes)

C. ROM Accuracy

For each ROM type, the number n of training samples was varied by powers of 2 from $n=2$ to $n=1024$. Each of the resulting models was then testing using the same $k=1000$ samples to evaluate each ROMs' accuracy. The root-mean-squared-error (RMSE) and normalized maximum error (Norm L_∞) of the most accurate of each ROM type are shown in Figure 11. One may see that for $n>200$, both the least-squares and SVD ROMs did not exhibit a reduction in error given further training samples. This was likely due to their limitation of their polynomial function order. However, the Kriging method continued to reduce in RMSE as additional training samples were added until $n=1024$ and was found to be the most accurate ROM approach of those considered. For all ROM types, a steady decline in the normalized L_∞ was observed and all ROM types showed approximately the same order of normalized L_∞ for $n>100$. Some minor noise was observed due to the random nature of the LHS method, but the overall trend that more training samples resulted in lower measures of error was clear.

D. ROM Computational Efficiency

Also critical to evaluation of a ROM's utility is the computational efficiency of a ROM. To quantify computational efficiency, the amount of computer memory the ROM must occupy and the time required for the ROM to be executed were considered. For each of the ROM types and training sets, the memory consumption and execution time required to run the $k=1000$ test samples was recorded and are shown in Figure 12. It can be seen that while the Kriging ROM was the most accurate, this accuracy came at the price of rapidly growing memory requirements

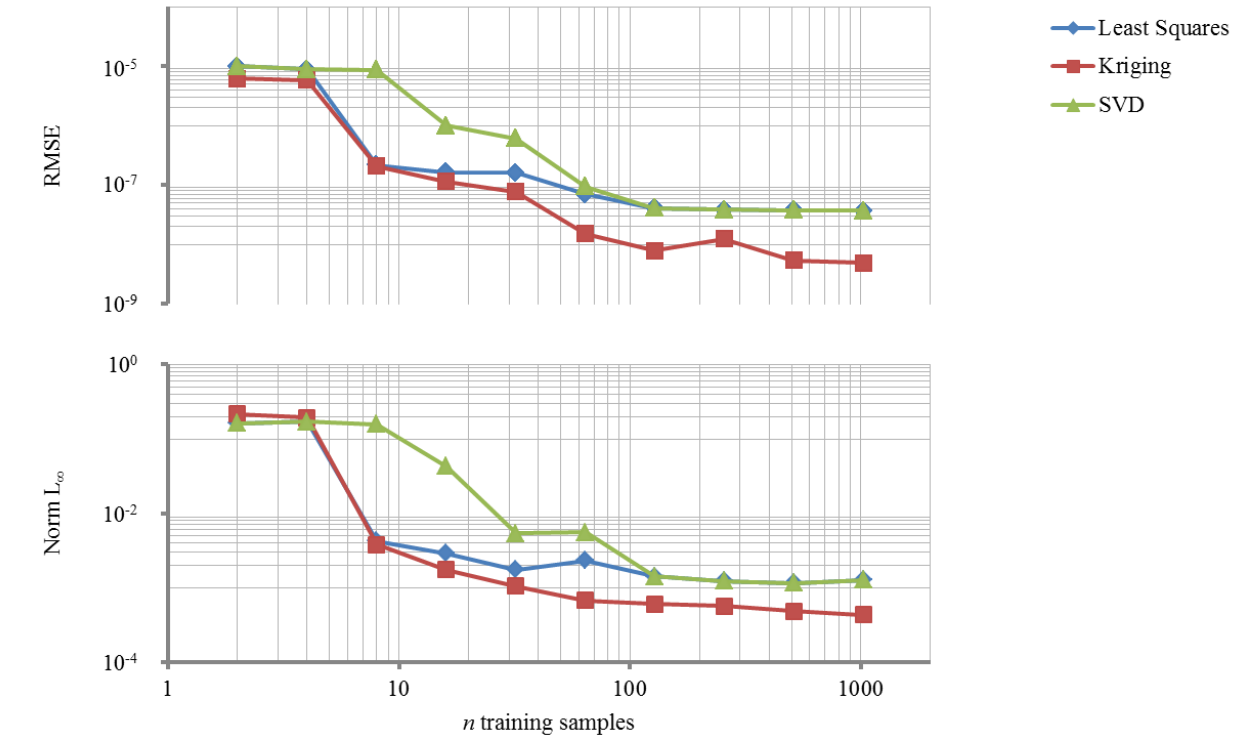

Figure 11: Effect of training sample size on the accuracy of ROMs generated from three different approaches

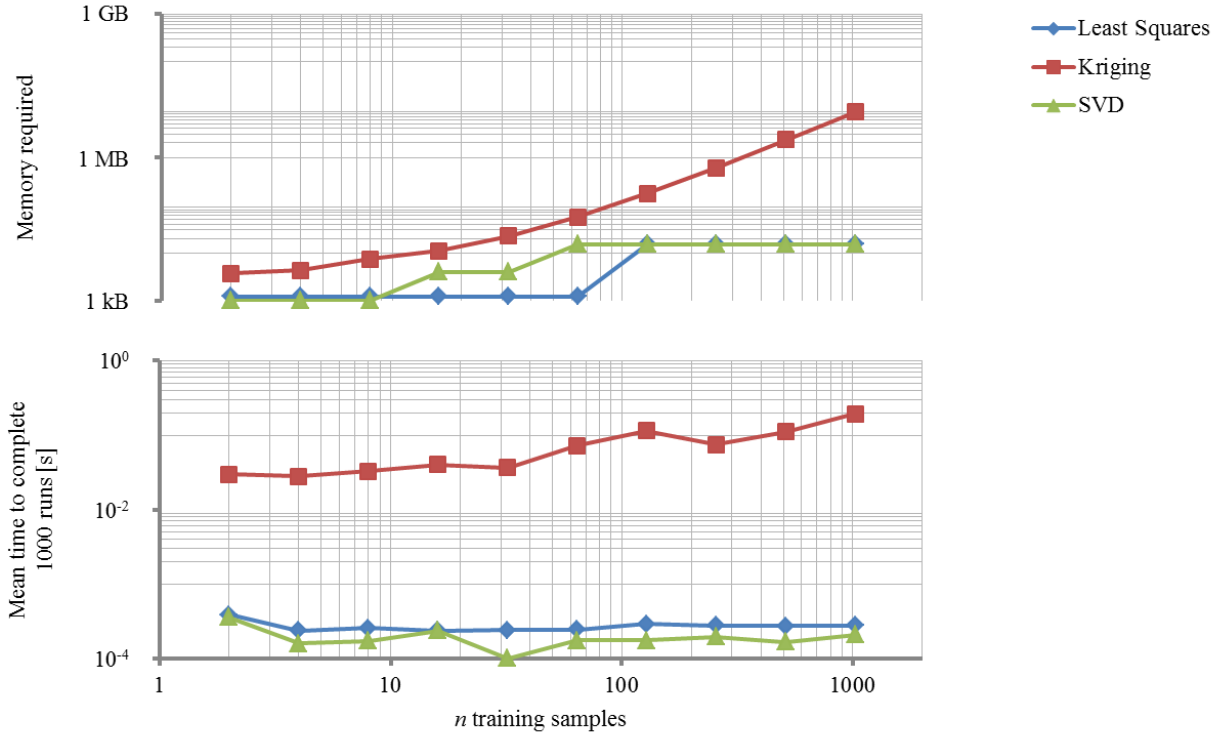

Figure 12: Effect of training sample size on the computational cost of ROMs generated from three different approaches

and slower execution times than the least-squares and SVD ROMs. This agreed with intuition since the method of Kriging is able to reproduce the entire training set and thus contains all of the information used to train the ROM. The least-squares and SVD approaches did not have the ability to reproduce the training set and thus retained only a fraction of the information used to train the ROMs which resulted in lower memory requirements for the computer.

In terms of processing speed, the least-squares and SVD ROMs were roughly 2 orders of magnitude faster than Kriging. The SVD ROM was also slightly faster than the least-squares ROM, however at these sub-millisecond scales, the specific implementation of the models and state of the computer's background programs may influence which of these two ROMs would be processed more quickly. To reduce random fluctuations in processing speed, each ROM was run 10 times, timed using the *tic* and *toc* functions of Matlab®, and the results averaged.

E. Comparison to FEA

As a final check of ROM accuracy, simulations of the generalized thermal problem with constant thermal properties versus with the SVD ROM were conducted. The constant thermal properties were taken from the materials at the mean temperature distribution observed during the FEA simulation. For both cases, the sample structure was started at a uniform 1260 K similar to the structure temperature at the initiation of the terminal phase of the trajectory. A steady outward heat flux was then applied with the spatial distribution

$$\dot{q} = -20341.7\left[\exp\left(-100x + 4\right)/10 + 0.9\right] \tag{14}$$

to simulate a cooling boundary layer with a logarithmic thickness profile. Here x is the distance in meters from the ballast edge furthest from the TPS and $\dot{q}$ is the heat flux in Watts per square meter. This is not physical since the boundary layer imposing the heat flux would change with the change in the wall boundary conditions; however the accuracy of the boundary layer heat flux is not the focus of this paper. Both thermal problems were integrated for 37.5 seconds, the duration of the terminal phase of the trajectory. The final temperature distributions for the FEA, 5-POD mode generalized system with constant thermal properties, and 5-POD mode generalized system with the SVD ROM varying the thermal properties can be seen in Figure 13. An overall improvement in the agreement between the FEA and 5-POD mode system solutions is evident when using the SVD ROM to model the thermal properties of the substructure. Compared to FEA, the 5-mode thermal system with constant thermal properties achieved a RMSE of 261.1 K while with the SVD ROM achieved 86.6 K.

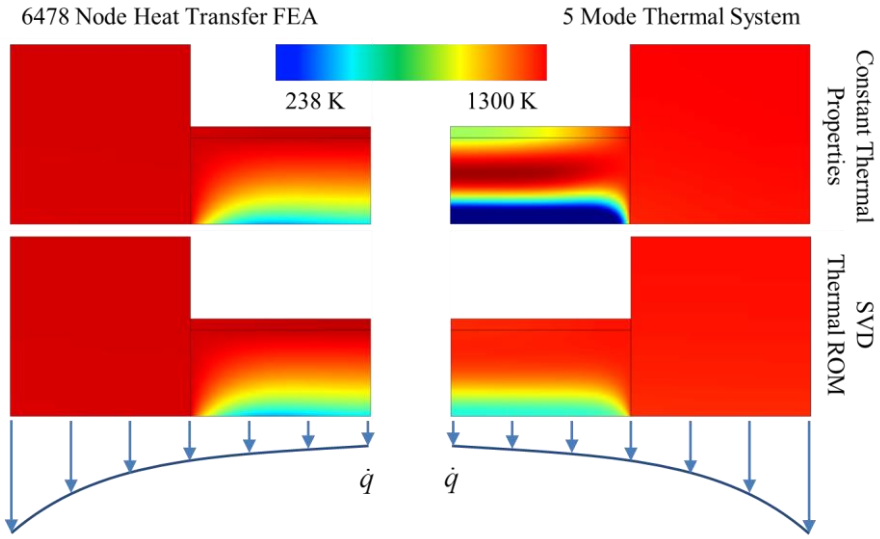

Figure 13: Significant qualitative improvement when using the SVD thermal ROM with the 5 mode thermal system compared to with constant thermal properties

V. Conclusions

Three reduced-order models were applied to the problem of modeling the thermal conductivity and capacity variation with respect to temperature for a sample substructure of a hypersonic vehicle. The thermal problem was first reduced through projection of the thermal states into bases determined by proper orthogonal decomposition. A relative error of order 10^{-8} was determined when the POD bases were truncated to the top 5 most prominent thermal modes. A Latin hypercube sample distribution of the thermal mode coordinates was then used to determine a sample set of generalized thermal conductivity and capacity matrices for the substructure. Various numbers of these samples were then used to create least-squares fit polynomial, Kriging, and singular-value decomposition based ROMs. These ROMs were then compared in terms of error compared to FEA solutions and numerical efficiency.

The SVD ROM was determined to be the superior approach. For relatively small training sample sizes of around 200, this ROM provided similar accuracy to the least-squares and Kriging methods. However, the SVD ROM also required up to ~600 times less memory than the Kriging ROM and was similar to the least-squares ROM. The SVD ROM was also capable of execution slightly faster than the least-squares ROM and roughly 100 times faster than the Kriging ROM.

Integration of the 5-mode generalized thermal problem was then performed with constant thermal properties and thermal properties varied according to the SVD ROM. Both generalized solutions were qualitatively compared to a full-order FEA solution with empirical thermal properties. Significant qualitative improvements were evident lending to the importance and utility of a thermal conductivity and capacity ROM for thermal problems spanning wide temperature ranges.

Acknowledgments

This work was sponsored by the Air Force Research Laboratory (AFRL), Munitions Directorate, Eglin Air Force Base, Florida. The technical monitor is Dr. Crystal Pasiliao. Opinions, interpretations, conclusions, and recommendations are those of the authors and are not necessarily endorsed by the United States Government.

References

[1]Falkiewicz, N.J, and Cesnik, C.E.S., "Proper Orthogonal Decomposition for Reduced-Order Thermal Solution in Hypersonic Aerothermoelastic Simulations," *AIAA Journal, Vol. 49, No. 5*, pp. 994-1009.

[2]Falkiewicz, N.J, and Cesnik, C.E.S., "Enhanced Modal Solutions for Structural Dynamics in Aerothermoelastic Analysis," *52nd AIAA/ASME/ASCE/AHS/ASC Structures, Structural Dynamics and Materials Conference*, Denver, Colorado, 2011, AIAA 2011-1963.

[3]McMasters, R.L., Zhou, Z., Dowding, K.J., Somerton, C., and Beck, J.V., "Exact Solution for Nonlinear Thermal Diffusion and Its Use for Verification," *Journal of Thermodynamics and Heat Transfer*, Vol. 16, No. 3, 2002.

[4]Matney, A.K., Mignolet, M.P., Spottswood, S.M., Culler, A.J., McNamara, J.J., "Thermal Reduced Order Model Adaptation to Aero-Thermo-Structural Interactions," *Proceedings of 55th AIAA/ASME/ASCE/AHS/ASC Structures, Structural Dynamics, and Materials Conference, January 2014, National Harbor, Maryland*, AIAA 2014-0493.

[5]Pasiliao, C.L., Sytsma, M.J., Neergaard, L.J., Witeof, Z.D., and Trolier, J.W., "Preliminary Aerothermal Structural Simulation", *Proceedings of the 14th AIAA Aviation Technology, Integration, and Operation Conference*, AIAA 2014-2292.

[6]Witeof, Z.D., and Neergaard, L.J., "Initial Concept 3.0 Finite Element Model Definition," *Air Force Research Laboratory*, Rept. AFRL-RWWV-TN-2014-0013, Eglin AFB, FL, April 2014. (96ABW-2014-0141).

[7]Trolier, J.W., Hall, D.W., Hudson, D.J., and Torres, M., "Aerothermal Targets Analysis Program (ATAP): Volume 2 – Engineering Document", SAIC-95/1022, 2004.

[8]Bialecki, R.A., Kassab, A.J., and Fic, A., "Proper Orthogonal Decomposition and Modal Analysis for Acceleration of Transient FEM Thermal Analysis", *International Journal for Numerical Methods in Engineering*, Vol. 62, No. 6, 2005, p. 774 – 797.

[9]Bialecki, R.A., Kassab, A.J., and Fic, A., "Reduction of the Dimensionality of Transient FEM Solutions Using Proper Orthogonal Decomposition," *Proceedings of the 36th AIAA Thermophysics Conference, June 2003, Orlando, Florida*, AIAA 2003-4207.

[10]Sacks, J., Welch, W.J., Mitchell, T.J., and Wynn, H.P., "Design and Analysis of Computer Experiments," *Statistical Science, Vol. 4, No. 4*, 1989, pp. 409-435.

[11]Manteufel, R.D., "Evaluating the Convergence of Latin Hypercube Sampling," *Proceedings of the 41st AIAA/ASME/ASCE/AHS/ASC Structures, Structural Dynamics, and Materials Conference and Exhibit, April 2000, Atlanta, Georgia*, AIAA 2000-1636.

[12]Crowell, A.R., and McNamara, J.J., "Model Reduction of Computational Aerothermodynamics for Hypersonic Aerothermoelasticity," *AIAA Journal, Vol. 50, No. 1*, 2012, pp. 74-84.

[13]Lillian, C.S., McDaniel, D.R., and Morton, S.A., "An Efficient Method of Computing Manuvering Aircraft Surface Loads Using CFD, Proper Orthogonal Decomposition, and System Identification," *Proceedings of the 49th AIAA Aerospace Sciences Meeting including the New Horizons Forum and Aerospace Exposition, January 2011, Orlando, Florida*, AIAA 2011-1177.

[14]Martin, J.D., "Robust Kriging Models," *Proceedings of the 51st AIAA/ASME/ASCE/AHS/ASC Structures, Structural Dynamics, and Materials Conference, April 2010, Orlando, Florida*, AIAA 2010-2854.

[15]Exelis, "Acusil® II Thermal Protection System," *Website: http://www.exelisinc.com/solutions/Acusil% 20_Thermal_Protection_System/Documents/ACUSIL_II_PR2013.pdf*, accessed 7 April 2015.

[16]Ohlhorst, C.W., Vaughn, W.L., Ransone, P.O., and Tsou, H., "Thermal Conductivity Database of Various Structural Carbon-Carbon Composite Materials," *Langley Research Center*, NASA Technical Memorandum 4787, 1997.

[17]Rehmer, B., Beckmann, J., Finn, M., and Glaubitz, S., "Determination of Elastic Moduli of C/C-Composite at Temperatures up to 1900C," *Federal Institute for Materials Research and Testing, Berlin, Germany*, 2004.

[18]Fitzer, E., and Manocha, L.M., "Carbon Reinforcements and Carbon/Carbon Composites," *Springer-Verlag Berlin Heidelberg*, 1998, pp.254-256.

[19]The Engineering Toolbox, "Young Modulus of Elasticity for Metals and Alloys," *Website: http://www. engineeringtoolbox.com/young-modulus-d_773.html*, accessed 7 April 2015.

[20]The Engineering Toolbox, "Metals – Specific Heats," *Website: http://www.engineeringtoolbox.com /specific-heat-metals-d_152.html*, accessed 7 April 2015.

[21]Allegheny Technologies Incorporated, "ATI Ti-6Al-4V, Grade 5, Technical Data Sheet," *ATI Documents Database* [online database], accessed 8 April 2015.

[22]Schmidt, F.F., and Ogden, H.R., "The Engineering Properties of Tungsten and Tungsten Alloys," *Defense Metals Information Center*, Columbus, Ohio, 1963, AD 425547.

[23]Klock, R.J., and Cesnik, C.E.S., "Aerothermoelastic Reduced Order Model of a Hypersonic Vehicle," *Proceedings of the AIAA Aviation Conference, June 2015, Dallas, Texas*, AIAA 2015-2711.

[24]Rexius, S.L., Rexius, T., Jorris, T.R., and Rao, A.V., "Advances in Highly Constrained Multi-Phase Trajectory Generation using the General Pseudospectral Optimization Software (GPOPS)", *Proceedings of the AIAA Guidance, Navigation, and Control (GNC) Conference*, AIAA 2013-4950.

[25]Abaqus FEM/CAE, Ver. 6.12, Dassault Systemes Simulia Corp., Providence, RI, 2012.

[26]Ashley, H. and Zartarian, G., "Piston Theory – A New Aerodynamic Tool for the Aeroelastician", *Journal of the Aeronautical Sciences, Vol. 23, No. 12*, 1956, pp. 1109-1118.

[27]Eckert, E.R.G., "Use of Reference Enthalpy in Specifying the Laminar Heat-Transfer Distribution Around Blunt Bodies in Dissociated Air", *Journal of Aerospace Sciences, Vol. 27, No. 6*, 1960, pp. 464-466.

[28]Golub G.H., and Kahan, W., "Calculating the Singular Values and Pseudo-Inverse of a Matrix", *Journal of the Society for Industrial and Applied Mathematics: Series B, Numerical Analyses, Vol. 2, No. 2*¸1965, pp. 205-224.

[29]Eglajs, V. and Audze, P., "New Approach to the Design of Multifactor Experiments", *Problems of Dynamics and Strengths, Vol. 35*, 1977, pp. 104-107.

[30]Hughes, T.J.R., "Unconditionally Stable Algorithms for Nonlinear Heat Conduction," *Computer Methods in Applied Mechanics and Engineering, Vol. 10, No. 2*, 1977, pp. 135-139.

[31]Lophaven, S.N., Nielsen, H.B., and Søndergaard, J., "DACE – A Matlab Kriging Toolbox," *Informatics and Mathematical Modeling*, Technical University of Denmark, 2002.